Pergamon

Journal of Structural Geology, Vol. 17, No. 9, pp. 1303 to 1318, 1995
Elsevier Science Ltd
Printed in Great Britain

0191-8141(95)00011-9

Strain accommodated by brittle failure in adjacent units of the Monterey Formation, U.S.A.: scale effects and evidence for uniform displacement boundary conditions

MICHAEL R. GROSS

Department of Geology, Florida International University, Miami, FL 33199, U.S.A.

and

TERRY ENGELDER

Department of Geosciences, Pennsylvania State University, University Park, PA 16802, U.S.A.

(*Received* 4 *January* 1994; *accepted in revised form* 14 *January* 1995)

Abstract—Extensional strain accommodated by brittle deformation was measured in adjacent mudstone and dolostone units at Arroyo Burro beach, California. The dolostone failed in effective tension whereas the mudstone failed in shear, both in response to the same extensional tectonic event. In the mudstone unit initial bed-length and fault-displacement methods document extensional strains of 6.6% ± 0.3% and 6.0% ± 0.3%, respectively. Upon adjusting the displacement estimates according to theoretical fault displacement population analysis, the corrected strain becomes 9.7% ± 0.3% for the mudstone. Measurements of vein apertures in the dolostone document extensional strain that varies according to scale, with outcrop vein scanlines indicating a strain of 3.4% ± 0.1%, and thin-section scanlines yielding a strain of 5.8% ± 0.2. Applying theoretical fault displacement population analysis to vein apertures in dolostone shows that small veins below the detection limit of outcrop surveys contribute significantly to fracture-related strain within the dolostone. This difference in extensional strain may arise because veins measured in outcrop extend across the entire bed height and thus are controlled by the dolostone mechanical layer thickness, whereas microscopic veins measured in thin-section terminate without regard to a bounding layer. The corrected dolostone strain becomes 10.2% ± 1.0%, matching the revised strain calculated in the adjacent mudstone unit and indicating uniform displacement boundary conditions for the two markedly different lithologies. The ~10% extensional strain at Arroyo Burro indicates significant strike-parallel (NW–SE) extension accommodated by brittle failure during development of the western Transverse Ranges fold and thrust belt.

INTRODUCTION

In sedimentary rocks composed of more than one lithology, deformation style may vary from one mechanical unit to the next. For example, in outcrops of the Monterey Formation exposed along the California coastline, opening mode veins and joints are commonly found in limestone, dolostone, and siliceous beds, whereas faults predominate in mudstones. Such a dependence of failure mode on lithology, herein referred to as *fracture partitioning*, creates a well-defined mechanical stratigraphy whereby opening mode fractures and faults are confined to separate mechanical units. For example, both the limestone and mudstone layers in Fig. 1 extended in response to the same applied remote stress conditions, yet the strain was accommodated by distinctly different failure processes.

Although a layered rock may be subjected to uniform regional tectonic stresses, the local fracture-related strain in each individual layer may be accommodated by distinctly different failure mechanisms. Therefore, characterizing relative magnitudes of extensional strain among mechanical units that fail in different modes may provide insight into the strain partitioning and deformation styles of layered rocks. For example, non-uniform displacement boundary conditions may occur during flexural slip folding and require a detachment between adjacent mechanical layers. Conversely, equal magnitudes of extensional strain must exist in cases such as Fig. 1 where adjacent beds are welded together.

This paper describes an analysis of extensional strain in adjacent mudstone and dolostone mechanical units of the Monterey Formation exposed along Arroyo Burro beach in Santa Barbara, California. We employ several techniques at different scales to measure extensional strain in the two mechanical units. We apply fault displacement population analysis to faults and veins in the mudstone and dolostone units, respectively, in order to attain revised strain estimates that account for unobserved extension. One goal is to determine whether uniform displacement boundary conditions apply to adjacent lithologies characterized by different failure modes. Displacement boundary conditions in turn provide key constraints for developing mechanical models to explain such phenomena as the relationship between failure mode and lithology as well as the correlation

between joint spacing and bed thickness. A second goal is to utilize strain and fracture spacing data to investigate the relationships between scale of observation, extensional strain estimates, and mechanical stratigraphy. Our third goal is to document the magnitude of NW–SE strike-parallel extensional strain accommodated by Pliocene to recent brittle deformation along the Santa Barbara coastline.

OUTCROP DESCRIPTION AND GEOLOGIC SETTING

A continuous cross-sectional exposure of the organic phosphatic member of the Miocene Monterey Formation extends for over 200 m along the coastline at Arroyo Burro beach in Santa Barbara, California (Fig. 2), affording an excellent opportunity to investigate relative magnitudes of extensional strain in adjacent mechanical units. Santa Barbara is located on the southern flank of the Santa Ynez Mountains, which comprises the western segment of the Transverse Ranges (Dibblee 1950). The western Transverse Ranges are interpreted as an actively developing fold and thrust belt characterized by fault-bend folding (Namson & Davis 1988, Shaw & Suppe 1994, Novoa *et al.* 1994). Regional north-northeast–south-southwest contraction began in the early Pliocene and persists until today as manifested by WNW oriented fold axes and faults (Reed & Hollister 1936, Dibblee 1982), active uplift and folding (Yeats 1983, Rockwell *et al.* 1988), and geodetically measured convergence (Savage *et al.* 1986, Larsen *et al.* 1993, Donnellan *et al.* 1993). Regional shortening corresponds to the NNE-SSW oriented maximum horizontal principal stress (S_H), which is documented by *in situ* stress measurements (Zoback *et al.* 1987), borehole breakouts (Mount 1989), and earthquake focal plane solutions (Yerkes 1985).

Outcrops of folded and intensely fractured Monterey Formation at Arroyo Burro are located on the southern flank of the faulted Mesa anticline (Hoyt 1976, Olson 1982, Hornafius 1994), south of the E–W-trending More Ranch and Lavigia faults (Fig. 2; Dibblee 1966, Olson 1982). Several episodes and styles of brittle deformation are present, including mechanically-confined joints, veins, and faults (i.e. fractures confined to discrete mechanical units; Gross 1993), along with faults and tar-filled vertical breccia zones that span the entire outcrop (Belfield *et al.* 1983, Gross in press, Hornafius 1994). We focus our study on two mechanical units at Arroyo Burro, a mudstone and a dolostone, which are distinguished from each other by virtue of their lithology and style of brittle deformation. The mudstone unit, a composite of several beds approximately 4.5 m in total stratigraphic thickness, consists dominantly of thick (100 cm) laminated organic phosphatic marl intervals interbedded with thin (5–20 cm) opal-CT layers. The bulk mechanical response of the mudstone unit to along strike extension is in the form of macroscopic faulting, with opal-CT beds faulting along with the rest of the mudstone unit, thereby providing excellent markers for measuring fault displacement (Fig. 3a). Individual opal-CT bed segments fail in effective tension and thus contain abundant opening mode fractures (Fig. 3b). Faults in the mudstone group lie in two apparent conjugate sets, with mean orientations of 238° 67° NW and 027° 50° SE (Fig. 4). Due to the lack of preserved slickenside lineations, we performed a geometric stress analysis assuming a conjugate fault origin and dip-slip motion on mean fault planes, where the σ_1 axis bisects the acute angle between the faults, σ_2 corresponds to the line of fault intersection, and σ_3 bisects the obtuse angle between faults (e.g. Ramsay & Huber 1983, Angelier 1994). The top of the mudstone unit is truncated by a late-formed subhorizontal fault.

A massive dolostone mechanical unit lies directly beneath the mudstone and consists almost entirely of fine-grained dolomite. Quantitative X-ray diffraction analysis yields a mineralogy consisting of 98% protodolomite, 1% quartz and 1% apatite. Beach sand covers the base of the dolostone unit, hence its thickness remains uncertain but is at least greater than 20 cm. In contrast to the mudstone unit, extension in the dolostone is accommodated by pure opening-mode veins oriented normal to the least principal stress (σ_3) at the time of propagation. Mean orientation for these strike-perpendicular veins is 234° 86° NW, and their extreme planarity is reflected in the tight cluster of poles on steroplots (Fig. 4). The direction of least principal stress inferred from the orientation of mudstone faults coincides precisely to the poles to strike-perpendicular veins found in the dolostone, consistent with the notion that the two styles of fracturing, restricted to different lithologies, developed concurrently. Identical relationships between σ_3 derived from faults in mudstone and the orientation of mode I fractures in adjacent units are found all along the Santa Barbara and Santa Maria coastlines (Gross in press), implying a genetic linkage between the two fracture styles. Extensional strain for both mudstone and dolostone mechanical units was measured along one-dimensional scanlines commonly oriented normal to the systematic strike-perpendicular vein set, at an azimuth of 144°. Based on their orientation, cross-cutting relationships, and planarity (i.e. lack of subsequent deformation), the veins and faults at Arroyo Burro probably represent northwest–southeast along-strike extension associated with development of the western Transverse Ranges fold and thrust belt during Pliocene to recent northeast–southwest directed contraction.

MUDSTONE EXTENSIONAL STRAIN

Two types of structural elements were measured in the mudstone in an effort to quantify extensional strain. The 'fault displacement' method involves measuring fault orientations and offset stratigraphic horizons to resolve horizontal displacement components parallel to the extension direction. The 'initial length' technique

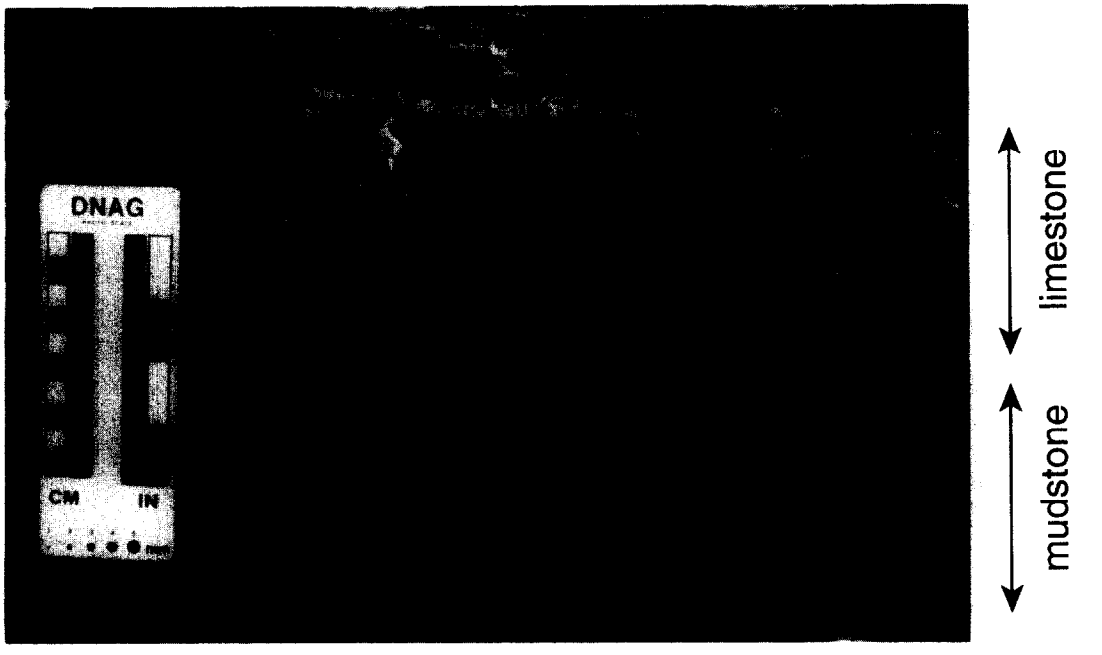

Fig. 1. Photograph of fracture partitioning in the Monterey Formation at Lion's Head, California. The light colored limestone layer in the upper half of the photo contains a series of ptygmatically-folded mode-I calcite veins that do not offset sedimentary laminae. Faulting characterizes brittle failure in the mudstone layer occupying the lower portion of the photo.

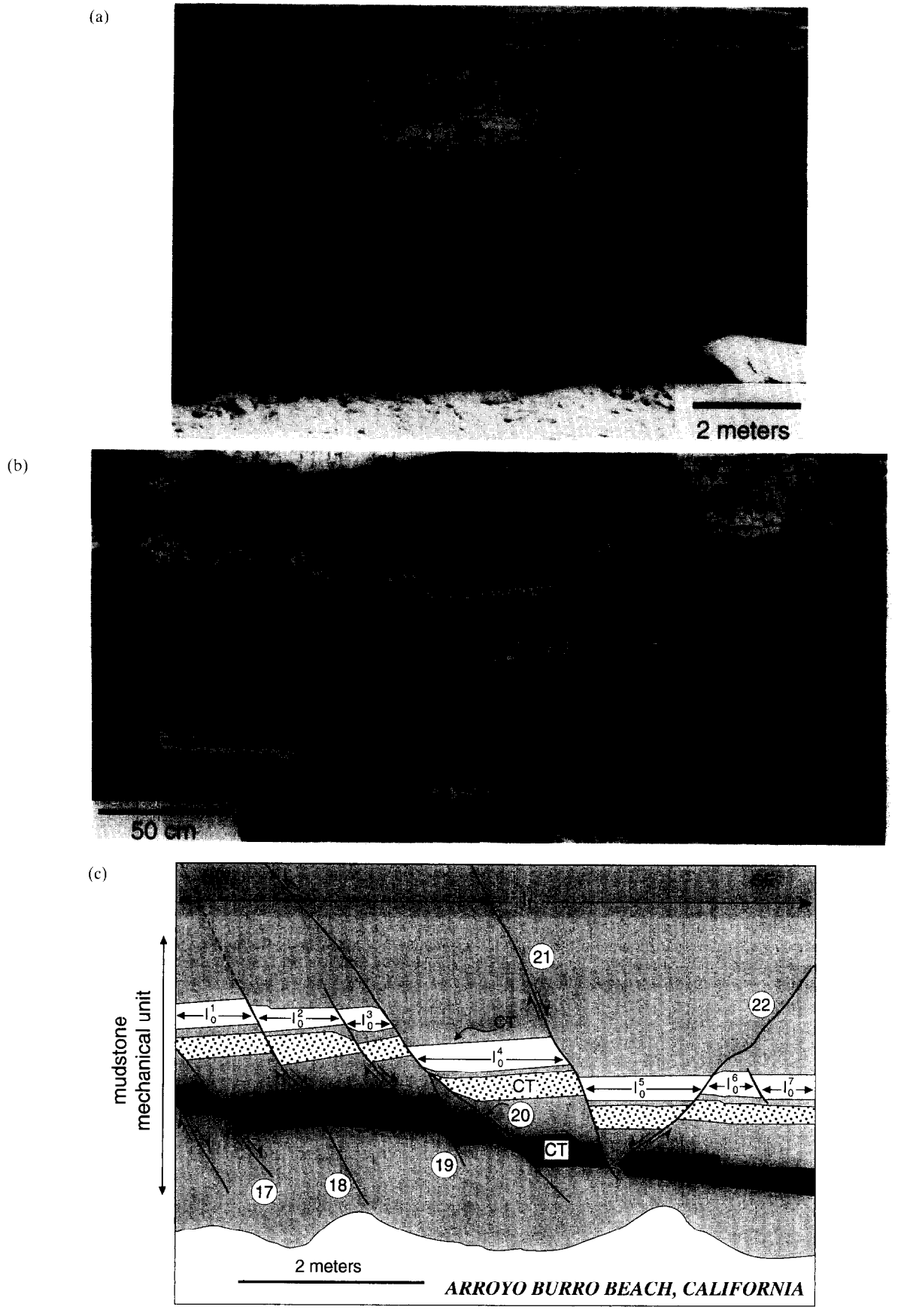

Fig. 3. (a) Photograph of macroscopic faults in a portion of the mudstone mechanical unit at Arroyo Burro beach. Light colored beds are siliceous opal-CT horizons and dark intervals are organic and phosphatic rich layers; (b) Close-up of central portion of Fig. 3(a) (note rock hammer) showing abundant opening-mode fractures in opal-CT horizons (arrows); (c) Sketch of Fig. 3(a). Extensional strain is measured by determining displacement across each fault, or by summing the original lengths (l_0) of opal-CT beds that fault along with the mudstone lithology. Numbers refer to faults in Table 1.

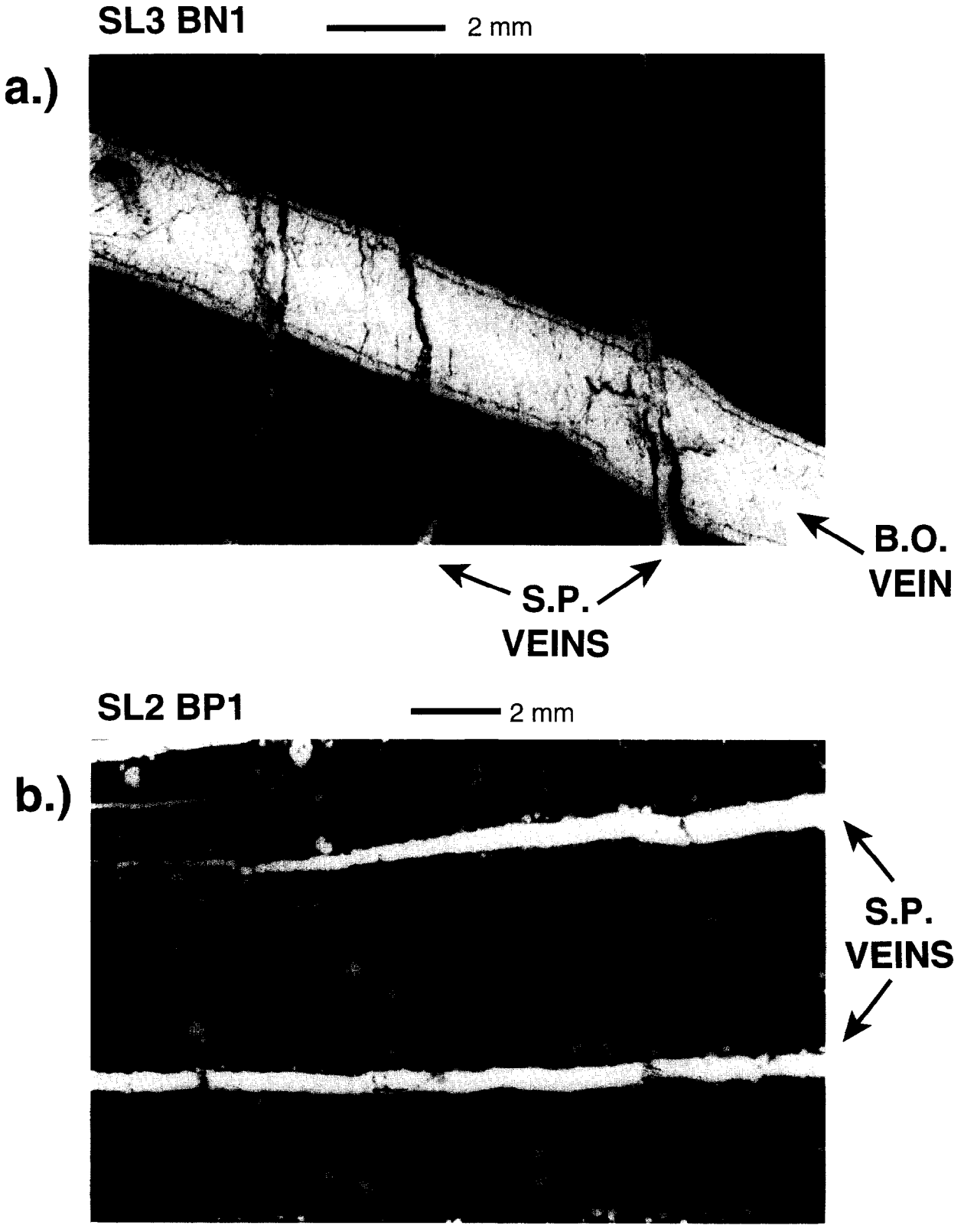

Fig. 9. Photomicrographs of systematic strike-perpendicular (SP) veins in the dolostone mechanical unit: (a) thin section cut normal to bedding showing the jagged nature and variable apertures of SP veins. Note also the SP veins post-date bedding oblique (BO) veins indicating their relative youth; (b) thin section cut parallel to bedding showing planar fracture wall geometry.

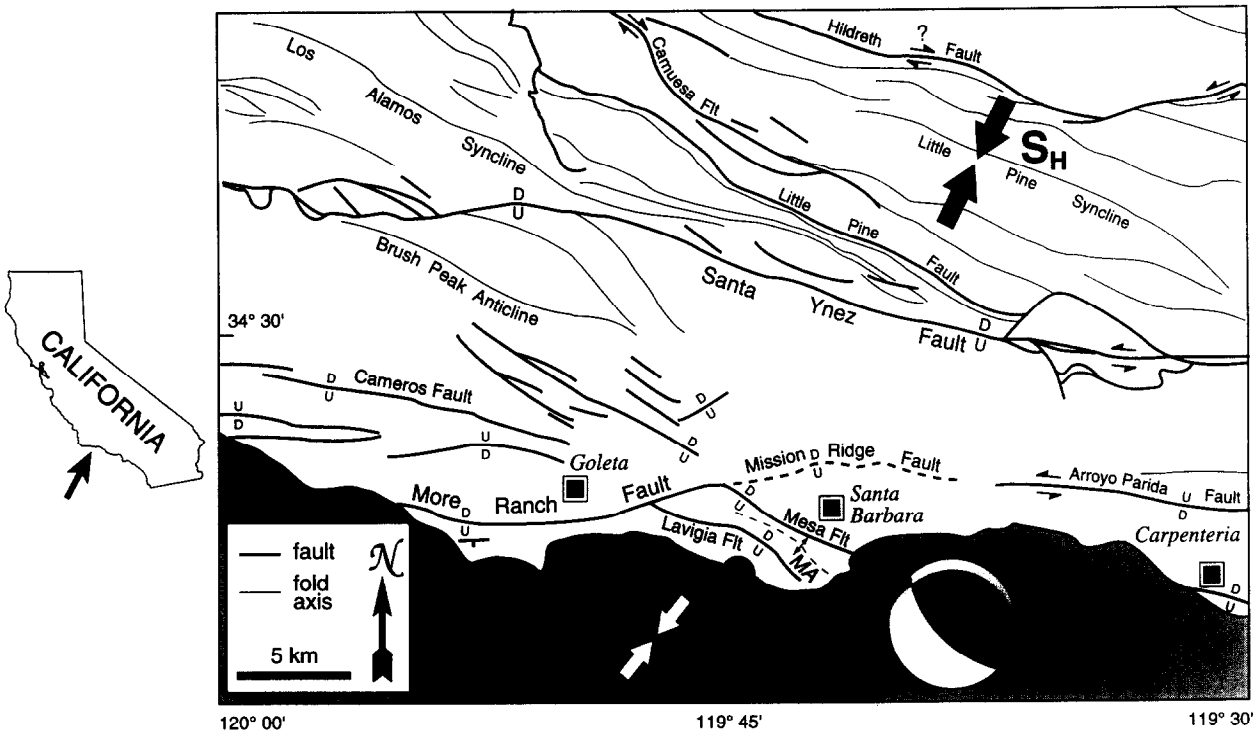

Fig. 2. Structure map of central Santa Ynez Mountains (after Dibblee 1966) showing location of Arroyo Burro section (ARR). Focal plane solution for the 1978 Santa Barbara earthquake (from Corbett & Johnson 1982) is plotted along with S_H trend (black arrows) derived from borehole breakouts (Mount & Suppe 1992) and structural trends. White arrows indicate local S_H at the time of conjugate shear failure in the mudstone unit at Arroyo Burro, which corresponds to the regional neotectonic stress configuration. *MA* refers to the Mesa anticline.

measures the same strain by summing the original segment lengths of opal-CT beds that fault along with the host mudstone lithology. The advantage of the fault displacement method is that a value of strain can be determined for the entire outcrop, though measurements of fault orientation and displacements are less accurate. The advantage of the initial length method is that bed lengths can be accurately measured, but only for limited intervals due to bedding attitude and exposure limitations. A portion of the mudstone scanline is presented as an outcrop sketch in Fig. 3(c), showing offset marker beds used to measure fault displacement as well as segments of an opal-CT layer representing original bed lengths.

Fault displacement method

A description of fault geometries and displacements for the 33 macroscopic faults encountered in the mudstone mechanical unit is presented in Table 1. Most of the faults measured along the 150 m scanline dip to the southeast with cross-sectional trace lengths ranging from 74 cm to over 600 cm. Smaller faults (5–10 cm in trace length) confined to organic-rich layers display minor displacements and appear as conjugate pairs, exhibiting orientations similar to the larger faults. These smaller faults do not extend into opal-CT beds, but rather accommodate thickening and thinning in the organic-rich horizons. The variety of macroscopic fault types include high-angle normal, listric normal, incipient normal with overlying drape folding, and vertical veins with up to 9 cm of opening-mode displacement. A majority of faults in the mudstone display a systematic decrease in displacement as they approach the underlying dolostone.

Extensional strain in the mudstone was calculated by resolving fault heaves (i.e. horizontal component of displacement) into the scanline direction. Fault displacement parameters were calculated for each of the 33 faults encountered in the mudstone mechanical unit (Table 1). The net contribution of each fault zone to the total fracture-related strain consists of the scanline-parallel displacement (ΔL_{SL}) plus any additional amount of material such as vein fill, fault gouge, and ductile flowing organic-rich sediments within the fault zone. Summing the net contributions of all the faults together results in a value of 843.4 cm for the total change in length of the mudstone (ΔL). The original length (L_0) is determined by subtracting the change in length (ΔL) from the scanline length (L_f), and the extensional strain (ε) in the scanline direction is calculated by dividing the change in length by the original length ($\Delta L/L_0$).

An overall extensional strain of 6.0% ± 0.31% was measured in the mudstone unit according to the fault displacement method (Table 2). The histogram presented in Fig. 5 demonstrates that scanline-parallel heaves for the 33 faults follow a power-law distribution, similar to the distributions of fault displacements and heaves reported by other workers (e.g. Kakimi 1980, Childs *et al.* 1990; Scholz & Cowie, 1990, Marrett & Allmendinger 1992, Walsh & Watterson 1992). One striking aspect of normal fault displacements at Arroyo Burro is that the majority of measured strain is accom-

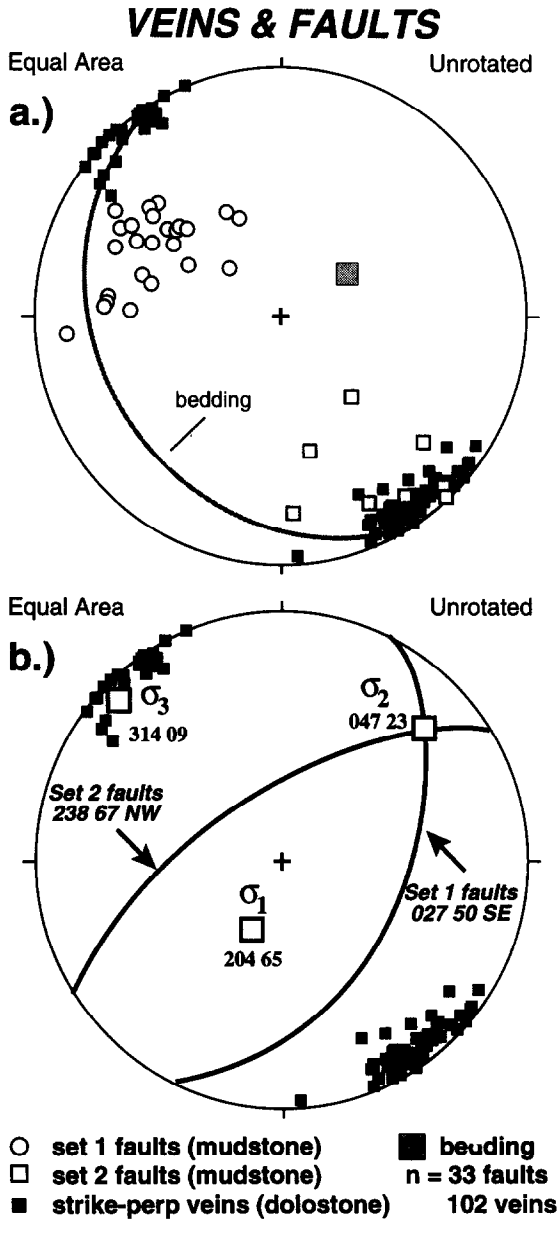

Fig. 4. (a) Stereoplot of poles to opening-mode veins in dolostone and faults in mudstone at Arroyo Burro. Note the tight clustering of veins and two conjugate fault sets. (b) Poles to opening-mode veins in dolostone along with principal stresses (trend and plunge) derived from mean mudstone fault sets at Arroyo Burro. Note the least principal stress (σ_3) falls within the cluster of poles to veins.

modated by a small number of faults. In fact, displacement across fault number 29 alone accounts for one third of the total extensional strain measured in the mudstone, and the seven largest faults (i.e. 20% of the faults) contribute 72% of that strain.

Initial length method

Three opal-CT beds within the dominantly organic phosphatic mudstone unit were selected at different localities along the mudstone outcrop for the 'initial length' strain analysis. Normal fault displacements resulted in segmentation of opal-CT beds during the extension process. Each fault-bounded section of an opal-CT bed shown in Fig. 3(c) defines an original length (l_0), such that for an opal-CT bed consisting of n segments, the initial bed length equals the sum of all its segments,

$$L_0 = l_0^1 + l_0^2 + l_0^3 + \cdots + l_0^n. \quad (1)$$

The scanline length represents the final length (L_f). The three measured opal-CT beds consist of 4, 24 and 9 individual segments with scanline lengths of 2400 cm, 5295 cm, and 3650 cm for beds 1, 2 and 3, respectively. Extensional strain for the three beds ranges from 6.0% to 7.0%, with an average of 6.6% ± 0.3% (Table 3). Because the opal-CT beds failed in effective tension in addition to being displaced by macroscopic faults, the 6.6% initial length extension measurement represents a minimum strain estimate which does not account for the presence of opening mode veins.

DOLOSTONE EXTENSIONAL STRAIN

Strain in the dolostone mechanical unit at Arroyo Burro was determined by measuring vein apertures on two scales. Outcrop scanlines provide extensional strain data from macroscopic structures whereas thin-section analyses yield data based on microscopic structures. The combined sum of vein apertures encountered along a scanline of final length (L_f) represents the change in length (ΔL) of the layer. Initial length equals the final length (L_f) minus the sum of vein apertures (ΔL). Therefore, in addition to comparing the magnitudes of strain between the mudstone and dolostone mechanical units, analysis of veins in the dolostone assesses the effect of scale on fracture strain estimates.

Outcrop vein measurements

Three outcrop scanlines combining for a total length of approximately 15.8 m were completed in the dolostone unit at different localities along the beach directly beneath the mudstone fault scanline. Apertures of 155 calcite veins belonging to the systematic strike-perpendicular set were measured using a vernier caliper, and 152 vein spacings were calculated as the perpendicular distance between adjacent veins along the scanline. These veins consistently terminate along the contact with the overlying mudstone unit, implying they are mechanically-controlled fractures extending across bed height (Gross 1993). Measured apertures of the planar strike-perpendicular veins range from a minimum of 0.1 mm up to 43.5 mm.

Strains for the three outcrop scanlines range from 2.7% to 5.8% (Table 2). The spatial clustering of veins, which results in an uneven vein distribution, may account for the wide range in strain estimates. For this reason the most representative estimate of macroscopic-scale strain for the dolostone outcrop scanline is obtained by combining data from all three scanlines and incorporating vein apertures over the total scanline length of approximately 15.8 m. The resulting 3.4% ± 0.14% estimate for extensional strain is noticeably less

Table 1. Fault geometries and displacements measured along extensional strain scanline in mudstone unit (organic-phosphatic marl member) at Arroyo Burro beach

Fault zone Number	Scanline distance (cm)	Fault type	Fault orientation	Displacement (cm)	ΔL_{DD} (cm)	ΔL_{SL} (cm)	Other extension (cm)	Total SL II extension (cm)
1	610	Incipient normal	235°/77°	8.0	1.80	1.80	7.0	8.8
2	1213	Incipient normal	028°/63°	4.0	1.82	1.64	0	1.64
3	2665	Vertical vein (Dn to E)	227°/89°	9.0	1.16	0.16	8.1	8.26
4a	3792	Normal	221°/66°	3.0	1.22	1.19	0	1.19
4b	3876	Normal	042°/57°	8.0	4.36	4.26	0	4.26
5	4107	Normal	258°/46°	65.0	45.15	41.25	4.1	45.35
6	4645	Normal	031°/60°	29.0	14.5	13.35	0	13.35
7	5980	Normal	032°/68°	8.0	3.0	2.78	0	2.78
8	6471	Listric normal	266°/68°	41.0	15.36	13.03	0	13.03
9	6988	Listric normal	016°/49°	13.0	8.53	6.72	0	6.72
10	7061	Normal	037°/55°	23.5	13.48	12.89	0	12.89
11	7625	Normal	042°/43°	12.0	8.78	8.59	0	8.59
12	7952	Normal	006°/60°	26.0	13.0	8.70	0	8.70
13	8485	Normal	062°/39°	71.0	55.18	54.64	0	54.64
14	8825	Normal	004°/60°	23.0	11.50	7.39	0	7.39
15	8832	Normal	244°/72°	10.2	3.15	3.10	0	3.10
16a	unclear	Normal	041°/45°	78.0	55.15	53.74	0	53.74
16b	9082	Normal	028°/35°	54.0	44.23	39.75	0	39.75
17	9147	Normal	039°/45°	29.0	20.51	19.81	0	19.81
18	9202	Normal	029°/50°	12.0	7.71	6.99	0	6.99
19	9345	Normal	033°/43°	17.5	12.80	11.95	0	11.95
20	9431	Normal	037°/48°	44.0	29.44	28.15	0	28.15
21	9547	Normal	022°/62°	56.0	26.29	22.30	0	22.30
22	9480	Listric normal	228°/36°	17.0	13.75	13.67	0	13.67
23	10,370	Low angle normal	042°/23°	61.0	56.15	54.92	0	54.92
24	10,389	Vertical	226°/85°	11.0	0.96	0.95	0	0.95
25	10,550	Normal	355°/76°	22.0	5.32	2.74	0	2.74
26	11,279	Normal	003°/61°	29.0	14.06	8.85	0	8.85
27	12,094	Normal	002°/51°	10.0	6.29	3.87	0	3.87
28	12,181	Normal	013°/45°	24.0	16.97	12.81	0	12.81
29	12,482	Normal (large)	067°/35°	342.0	280.15	272.97	0	272.97
30	13,110	Normal	027°/55°	150.5	86.32	76.91	0	76.91
31	13,657	Normal	039°/58°	24.0	12.72	12.29	0	12.29
END Scanline @ 15000 cm							**Total**	**843.36**

ΔL_{DD} = horizontal displacement in dip direction; ΔL_{SL} = horizontal displacement in scanline direction; other extension includes fault gouge and vein aperture; Total SL ‖ = total scanline parallel extension; fault orientations according to right-hand rule.

Table 2. Summary of strain estimates measured at Arroyo Burro according to the four techniques employed, along with revised strain estimates based on theoretical fault displacement population analysis

SL number	ΔL aperture (cm)	L_f final length (cm)	L_o L_f–ΔL initial length (cm)	ε (%) $\Delta L/L_o$ extension	Number of veins, faults, segments	Revised strain (%)
Outcrop veins						
1	21.61	816.0	794.39	2.7	71	
2	15.11	273.5	258.39	5.8	34	
3	16.04	490.0	473.96	3.4	50	
Total	**52.76**	**1579.5**	**1526.74**	**3.4 ± 0.14**	**155**	
Thin section veins		**Average**		**5.8 ± 0.2**	**513**	**10.2 ± 1.0**
Normal faults	**843.36**	**15,000.00**	**14,156.64**	**6.0 ± 0.31**	**33**	**9.7 ± 0.31**
Initial bed length				**6.6 ± 0.30**	**37**	

than the 6.0% ± 0.31% to 6.6% ± 0.30% estimates in the mudstone mechanical unit.

A generally skewed, though multimodal, log–normal distribution of vein spacing (Fig. 6) resembles spacing distributions of opening-mode fractures confined to mechanically layered rocks (e.g. Huang & Angelier 1989, Narr & Suppe 1991, Gross 1993). Vein apertures are combined into histograms in Fig. 7. The histogram in Fig. 7(a) spans the entire range of vein apertures, including the very wide 43.5 mm vein, and clearly shows a power-law distribution. Upon limiting the range from 0 to 20 mm the power-law trend remains, however the smallest class interval (0–1 mm) appears underrepresented (Fig. 7b). A similar type of sampling truncation was reported by Segall & Pollard (1983) for fracture lengths measured in granodiorites of the Sierra Nevada. The undersampling of veins less than 1 mm wide presents an obvious limitation to the outcrop-scale dolostone strain analysis. Furthermore, unlike the mudstone mechanical unit where displacement across only a few faults accounts for the majority of extension, the aperture of the largest vein represents only 8.2% of the total horizontal displacement measured in the dolostone. Therefore, the relatively low 3.4% extensional

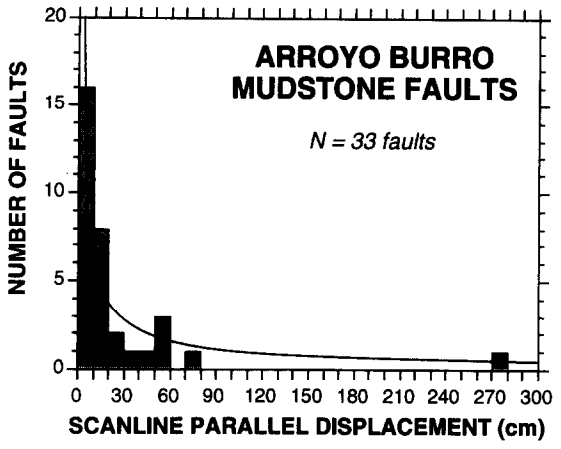

Fig. 5. Histogram of heaves (i.e. scanline parallel displacement) for faults in the mudstone mechanical unit with power law curve fit.

strain estimate derived from outcrop dolostone scanlines may indeed reflect the omission of smaller veins, which could contribute significantly to the overall strain.

Thin-section vein measurements

Two thin-sections each, one cut normal (BN) and the other parallel (BP) to bedding were prepared from two large samples collected at dolostone scanlines 2 (SL2) and 3 (SL3). Extensional strain was determined by measuring vein apertures from collages of photomicrographs. Veins appear less planar in thin-section than in outcrop, and in addition to smaller veins frequently pinching in and out, larger veins often exhibit wide variations in aperture along their lengths. Therefore, in order to achieve representative strain estimates, an average strain was calculated from a series of six or seven parallel traverses conducted along each thin-section (Fig. 8). In thin-section, vein walls characteristically appear more planar when observed parallel to bedding than perpendicular to bedding (Fig. 9).

Twenty-five traverses were conducted across the four thin-sections, combining for a total of 513 aperture measurements (Table 4). Thin-section apertures range from 0.013 mm to 0.93 mm, overlapping the range measured in outcrop. Average scanline strains for the four thin-sections are 5.23% for SL2 BP1, 5.68% for SL2 BN2, 6.14% for SL3 BP1, and 5.95% for SL3 BN1. Consistent strain values were derived from the four thin-sections; though measured strains are slightly higher in the SL3 samples, all mean values fall approximately within the range of error (Fig. 10).

Vein aperture measurements, presented as histograms divided into class intervals of 0.05 and 0.025 mm, follow a power-law distribution (Fig. 11). Similar to outcrop aperture measurements, the smallest class interval in Fig. 11(b) appears undersampled, however, as demonstrated in the following sections, their contribution to the overall strain is less significant. In addition, the fact that thin section and outcrop vein aperture populations overlap indicate that several outcrop scale veins extending across the entire mechanical layer were measured in thin section (Fig. 11). Spacing histograms for veins measured in thin section (Fig. 6b,c) reveal distributions resembling power-law functions, which are significantly different from the log–normal function describing outcrop vein spacing (Fig. 6a).

Two possible explanations exist for the 70% greater extensional strain measured at thin-section scale. One is that thin sections overestimate the strain because they do not adequately represent the rock mass; whereas macroscopic surveys total over 15 m of outcrop length, thin sections account for less than 20 cm. Thus, vein clustering and anti-clustering (i.e. larger intervals without veins) will result in severely biased strain estimates. The second explanation for the discrepancy is that small veins, below the detection limit of outcrop surveys, contribute significantly to the overall extensional strain within the dolostone unit. Aperture population curves presented in the following section provide overwhelming evidence in favor of the second explanation.

DISPLACEMENT POPULATION ANALYSIS APPLIED TO ARROYO BURRO MECHANICAL UNITS

Calculating extension by summing observed fault displacements commonly underestimates total strain by failing to account for the contribution of small unobserved faults (e.g. Angelier 1985, King & Cisternas 1991, Marrett & Allmendinger 1991, Walsh *et al.* 1991). A quantitative method based on the observed power-law distribution of fault displacements, referred to as theoretical fault displacement population analysis (TFDPA), allows for an estimation of total strain from inherently limited sample populations. Fault displacement populations often obey a power-law distribution such that

$$N \simeq d^{-C} \tag{2}$$

where N is the total number of faults with displacements greater than or equal to d (e.g. Childs *et al.* 1990, Scholz & Cowie 1990, Marrett & Allmendinger 1992). The exponent C characterizes the relative abundances of large and small faults, and represents the negative slope of linear segments on log–log plots in cases where fault displacement populations follow fractal distributions (Marrett & Allmendinger 1992).

Marrett & Allmendinger (1992) derive an expression to calculate the amount of extension accommodated by small-scale faulting. The total one-dimensional extension (ΔL) equals the sum of all fault heaves:

$$\Delta L \cong h_1 + h_2 + h_3 + \cdots + h_N + h_e, \tag{3}$$

where h_1 is the heave of the largest fault, h_2 is the heave of the second largest fault, and h_e equals the sum of heaves for incompletely sampled faults. N is the number and h_N is the heave of the smallest fault in the range over which sampling of the fault population is complete. The contribution of incompletely sampled faults to the total extension is:

Table 3. Extensional strain in the mudstone mechanical unit at Arroyo Burro determined from measurements of opal-CT bed lengths

Bed number	Location	n Number of segments (cm)	$L_0 = \sum_1^n l_0^n$ Initial length (cm)	L_f Final length (cm)	ΔL $L_f - L_0$ (cm)	ε $\Delta L/L_0$
1	FZ#5–#7	4	2265	2400	135	6.0
2	FZ#12–#26	24	4947	5295	348	7.0
3	FZ#30–#31	9	3421	3650	229	6.7
Average						**6.6**

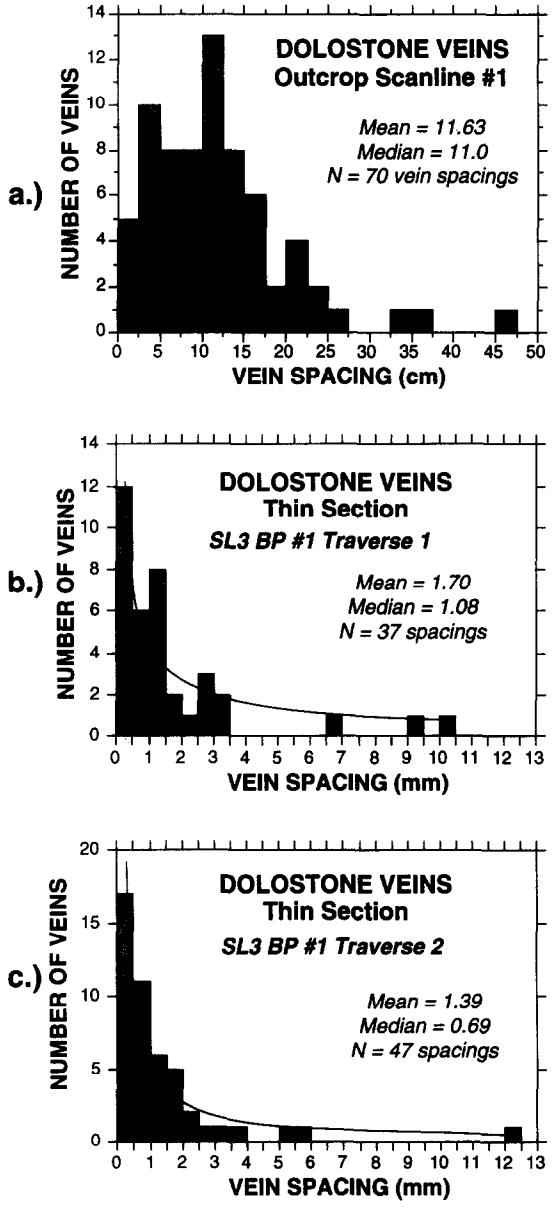

Fig. 6. Vein spacing histograms from the dolostone mechanical unit: (a) Macroscopic vein spacing from dolostone outcrop scanline # 1; (b) & (c) Microscopic vein spacings in thin section with power law curve fits.

$$h_e = h_N \frac{C}{1-C}(N+1)\left(\frac{N}{N+1}\right)^{1/C}. \qquad (4)$$

The expression for h_e converges only for values of C less than 1, thus equation (4) cannot be used to estimate strain for $C \geq 1$. The lower the value of C, the greater the contribution of larger faults to the total strain, whereas

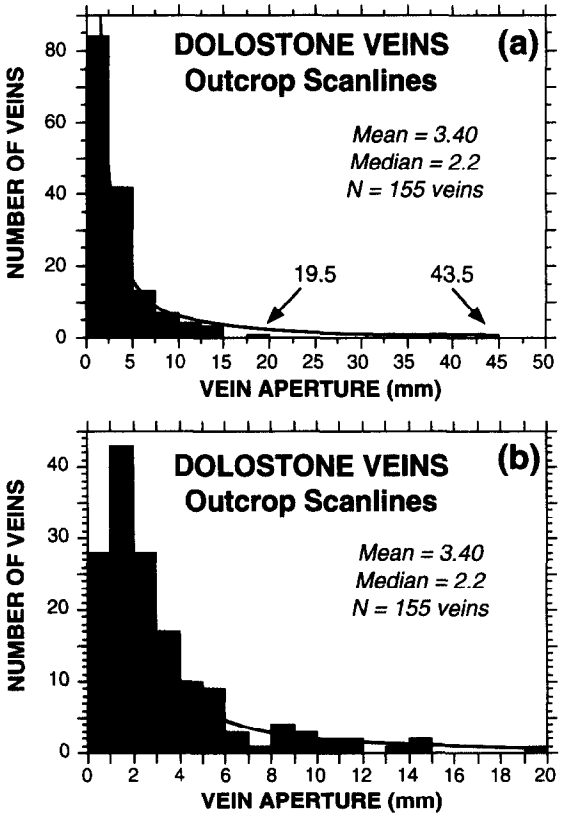

Fig. 7. Histogram of macroscopic vein apertures from combined dolostone scanlines for ranges 0–50 mm (a), and 0–20 mm (b) along with power law curve fits.

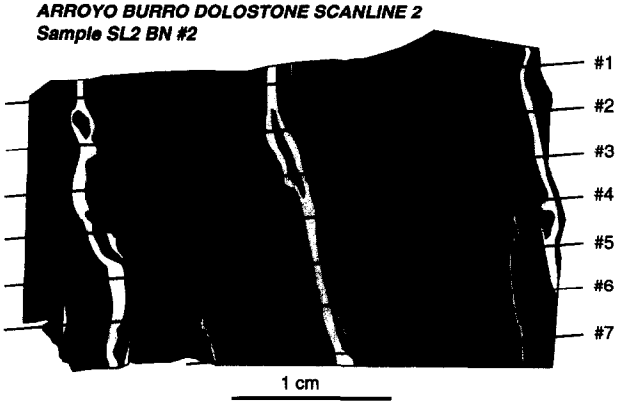

Fig. 8. Sketch of thin section cut normal to bedding from dolostone scanline # 2 at Arroyo Burro. Extensional strain was measured along a series of parallel traverses perpendicular to the mode I veins (see Table 4 for strain data).

Table 4. Extensional strain measured in thin section from dolostone beds at Arroyo Burro. Extension (ΔL) represents the sum of all apertures measured along a traverse. BN refers to thin sections cut normal to bedding and BP refers to thin sections cut parallel to bedding. Thin sections were prepared from samples taken from outcrop dolostone scanline 2 (SL2) and scanline 3 (SL3). C is the slope of the vein aperture population curve, which was not calculated for SL2 due to low sample numbers. Revised strain estimates were derived using theoretical fault displacement population analysis

Thin section	Traverse	ΔL Σ aperture (mm)	L_f Final length (mm)	L_0 $L_f-\Delta L$ Initial length (mm)	$\varepsilon(\%)$ $\Delta L/L_0$ strain	Number of veins	C	Revised Strain
ARR St 7 SL2 BP#1	1	2.493	59.24	56.747	4.39	16		
	2	2.801	59.06	56.259	4.98	14		
	3	2.528	58.80	56.272	4.49	12		
	4	3.044	58.72	55.676	5.47	12		
	5	3.166	57.20	54.034	5.86	11		
	6	3.183	54.42	51.237	6.21	10		
	Average				**5.23**			
ARR St 7 SL2 BN#2	1	1.661	31.92	30.259	5.49	11		
	2	2.333	32.96	30.627	7.62	7		
	3	2.038	32.70	30.662	6.65	8		
	4	2.120	33.04	30.920	6.86	8		
	5	1.726	33.65	31.924	5.41	6		
	6	1.596	32.26	30.664	5.20	5		
	7	0.559	22.64	22.081	2.53	4		
	Average				**5.68**			
ARR St 7 SL 3 BP#1	1	3.465	69.73	66.265	5.23	38	na[1]	na
	2	3.677	69.56	65.883	5.58	48	0.82	13.9
	3	3.816	70.16	66.344	5.75	32	0.67	8.7
	4	4.549	70.16	65.611	6.93	39	0.69	10.8
	5	4.105	68.65	64.635	6.21	34	0.85	16.5
	6	4.662	69.86	65.198	7.15	38	0.76	12.1
	Average				**6.14**			
ARR St 7 SL 3 BN#1	1	2.897	63.31	60.413	4.80	22	0.54	6.0
	2	3.322	64.18	60.858	5.46	29	0.54	6.4
	3	3.040	63.31	60.270	5.04	22	0.81	13.3
	4	4.562	61.58	57.018	8.00	39	0.45	9.4
	5	3.161	56.20	53.039	5.96	23	0.48	6.9
	6	3.018	49.78	46.762	6.45	25	0.48	7.8
	Average				**5.95**			

[1] na = TFDPA not applicable.

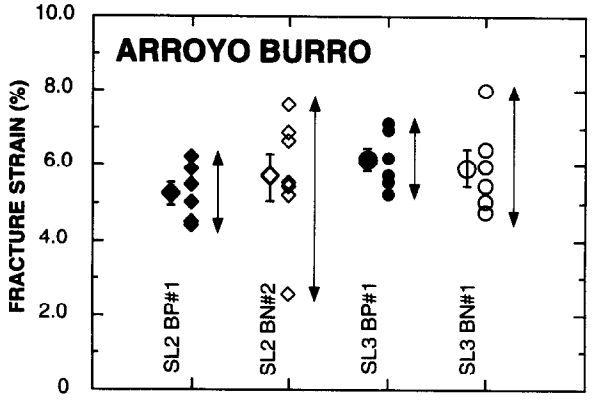

Fig. 10. Fracture strain measurements for four thin sections from dolostone scanlines # 2 and # 3 (i.e. SL2 and SL3). Thin sections were cut parallel (BP) and normal (BN) to bedding. Mean values are presented alongside individual traverse strain measurements. Note the consistent mean strain values derived from all sections, yet the wider range in strains (arrows) recorded in bedding normal sections. Bars represent standard error.

high C values indicate that smaller faults provide significant contributions to the net strain.

A summary of initial strain estimates calculated from the four methods employed at Arroyo Burro are presented in Fig. 12. The two structural elements employed to measure strain in the mudstone unit, the initial length and fault displacement methods, yield overlapping extensions of 6.6% ± 0.3% and 6.0% ± 0.31%, respectively. Whereas outcrop vein measurements in the dolostone unit indicate 3.4% ± 0.14% strain, analysis of vein apertures in thin-section yields a substantially higher strain of approximately 5.8% ± 0.2%. In the following section TFDPA is applied to both mechanical units at Arroyo Burro in order to estimate true strain and compare relative magnitudes of along-strike extension.

Revised strain estimate for the mudstone mechanical unit

A displacement population plot representing measured offsets along the 33 faults encountered in the mudstone mechanical unit is shown in Fig. 13(a). Central linear segments for all displacement and aperture population plots were determined by visually identifying breaks in slope and matching the highest linear correlation coefficient. The value of 0.75 for C derived from the slope of the linear central segment indicates that large faults accommodate most of the total strain, and small faults below the limit of resolution account for only a small portion. According to Marrett & Allmendinger's (1992) equations:

$$\Delta L = 822.9 + h_e. \quad (5)$$

Using the total scanline parallel extension from Table 1 as the displacement input parameter, the smallest measured extension (h_N) equals 6.72 cm. Inserting

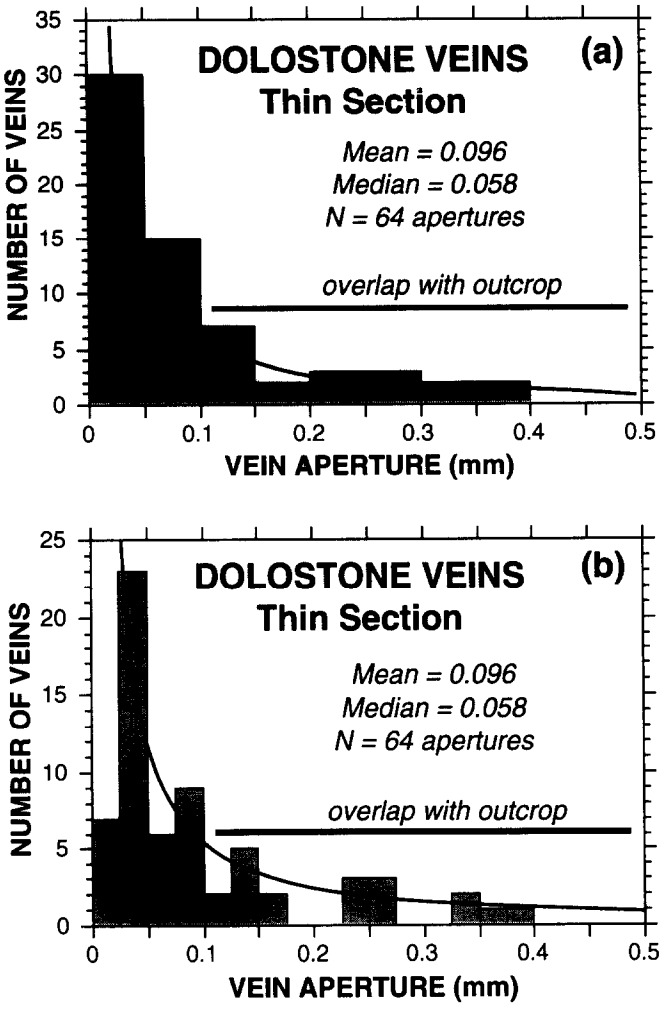

Fig. 11. Vein aperture histograms for dolostone thin sections divided into class intervals of 0.05 mm (a) and 0.025 mm (b) along with power law curve fits. Aperture data were combined from SL2 BP#1 T1 and SL3 BP#1 T2.

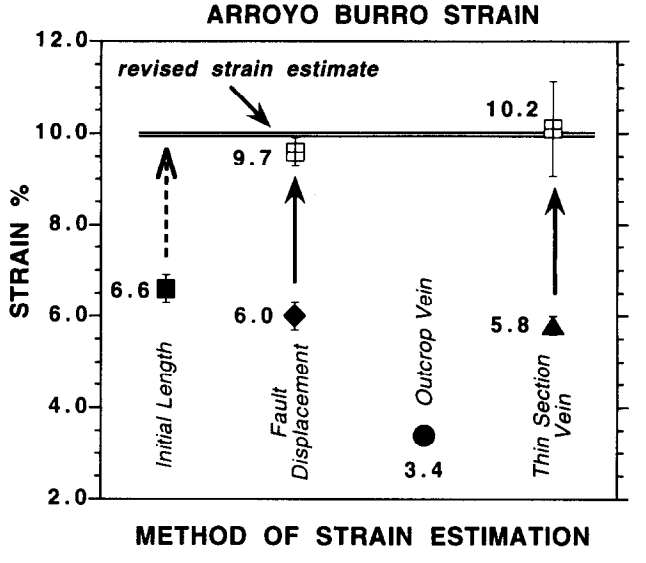

Fig. 12. Summary of strain estimates for the four methods exployed at Arroyo Burro. Solid symbols refer to initial strain estimates and white squares accompanied by black arrows denote revised strains based on TFDPA. Note the nearly identical revised extension estimates for mudstone and dolostone units. Dashed arrow refers to the amount of strain accommodated by opening-mode fracturing in individual opal-CT segments. Error bars from Table 2.

values of 0.75 for C, 25 for N, and 6.72 for h_N into equation (4) results in a value of 499 cm for h_e, which represents the sum of heaves for the small unobserved faults. Therefore, the true total extension is approximately 1322 cm, and the amount of extension originally estimated from the faults at Arroyo Burro represents 64% of the true extension. Thus the revised strain estimate in the mudstone unit according to the fault displacement method equals 9.7% ± 0.3 (Fig. 12). Based on this revised total strain calculation, the amount of extension accommodated by mode I fracturing in individual opal-CT beds located within the mudstone unit equals 9.7% – 6.6%, or ~3.1% (dashed arrow in Fig. 12).

Revised strain estimate for the dolostone mechanical unit

Vein aperture population data from the dolostone mechanical unit reveal an intriguing dependence of C on the scale of observation. Macroscopic vein apertures measured in outcrop, which yield the lower strain estimate of 3.4%, display a value for C of 1.37 (Fig. 13b). Such a high C value implies that small veins below the limit of detection account for a substantial portion of the total dolostone extension, and hence the 3.4% strain estimate is much less than the true strain. The same conclusion was reached through inspection of macroscopic vein aperture histograms (see Fig. 7) and born out by the study of microscopic vein apertures. A revised strain estimate based on macroscopic vein apertures cannot be derived using equation (4) because $C > 1$.

The population distribution technique applied to veins in thin-section yields markedly different results. In contrast to the outcrop vein apertures, all of the C values derived from thin-section traverses are less than 1. Values of C for traverses from thin sections SL3 BP1 and SL3 BN1, selected for analysis because each contains a minimum of 22 measurements, range from 0.45 to 0.85 (Table 4). Examples of thin-section graphs presented in Figs. 13(c) & (d) exhibit central linear segments typical of fault displacement population plots. Revised strain calculations based on equation (4) for thin-section traverses yield a mean dolostone extensional strain of 10.2% ± 1.0, overlapping the revised 9.7% ± 0.31% extension measured in the overlying mudstone unit (Fig. 12). The mean dolostone strain was determined by averaging strains calculated independently for each traverse. Because the calculation for thin-section strain includes contributions from outcrop scale veins (see Fig. 11), the 10.2% strain estimate based on thin-section apertures represents a cumulative strain for all scales of veins in the dolostone mechanical unit.

DISCUSSION

Three major points arise from the application of fault displacement population analysis to the mudstone and dolostone mechanical units at Arroyo Burro. First, upon adjusting strain estimates to account for undetected

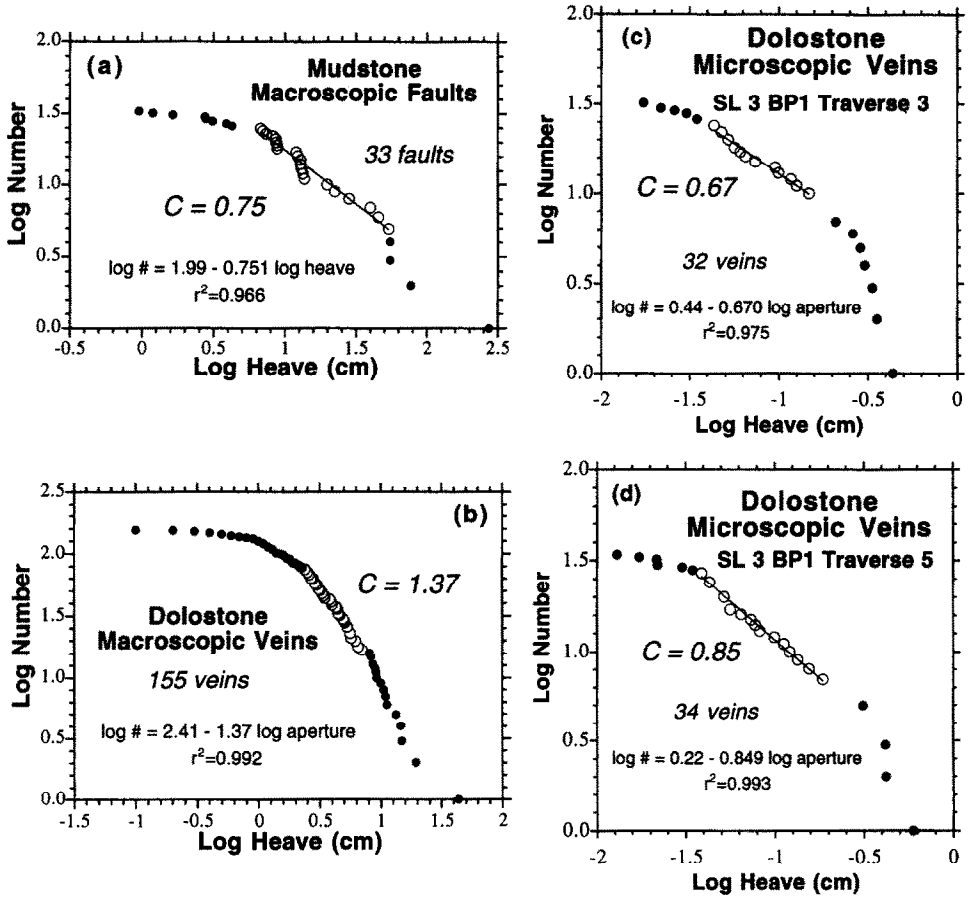

Fig. 13. Theoretical fault displacement population plots from Arroyo Burro for: (a) macroscopic extension faults in the mudstone; (b) macroscopic veins in dolostone; (c) & (d) microscopic veins in dolostone.

faults and veins, values of approximately 10% extensional strain were calculated for both mechanical units. Such uniform displacement boundary conditions accommodate deforming packages of beds within the Monterey Formation that are welded together along their contacts. Second, by virtue of its high C value, the relatively low 3.4% extensional strain determined from dolostone outcrop vein apertures is an underestimate caused by limited visual resolution, and does not provide an accurate assessment of true strain in the dolostone. Thin-section vein scanlines, on the other hand, yield significantly lower C values and provide more reliable cumulative dolostone strain estimates by accounting for extension accommodated by unobserved small veins. Third, the fact that both vein spacing and aperture population distributions in the dolostone unit vary significantly according to scale implies that mechanical stratigraphy plays a key role in vein set development.

Mechanical controls and scale effects

The dependence of failure mode on lithology in the Monterey Formation is manifested by markedly different brittle deformation mechanisms in adjacent units: faulting in mudstone and mode I veining in dolostone. Though magnitude of along-strike strain is identical for both layers, large faults account for the bulk of extension in the mudstone while microscopic mode I veins make an important contribution to the dolostone strain. Mechanical controls on the brittle deformation process may explain this difference, with scale playing an important role in the dolostone whereas stratigraphic distance between adjacent opal-CT layers exerts an influence on the extension process in the mudstone.

On the outcrop scale vein spacing in the dolostone follows a log–normal distribution typical of well-developed, bedding-confined (i.e. mechanically layered) joints (Fig. 6a; Huang & Angelier 1989, Narr & Suppe 1991, Gross 1993), while vein spacing in thin-section appears to follow a negative exponential or power-law trend similar to joints found in crystalline (i.e. massive, non-layered) rocks (Figs. 6b & c; Segall 1981). Different distributions may arise because veins measured in outcrop consistently terminate at the boundary defined by the mudstone lithologic contact, whereas most of the microscopic veins terminate at various locations within the massive dolostone (Fig. 14). Thus on a macroscopic scale, veins in the dolostone are controlled by a mechanically layered medium with vein height equal to bed thickness (i.e. mechanically-confined veins), hence the log–normal spacing distribution. Conversely, microscopic veins behave as if in a massive homogeneous medium, with veins terminating at various localities within the rock mass and vein height much less than mechanical layer thickness, resulting in a power-law or negative exponential spacing distribution. Markedly different vein spacing distributions at thin-section and outcrop scales in the dolostone parallel the

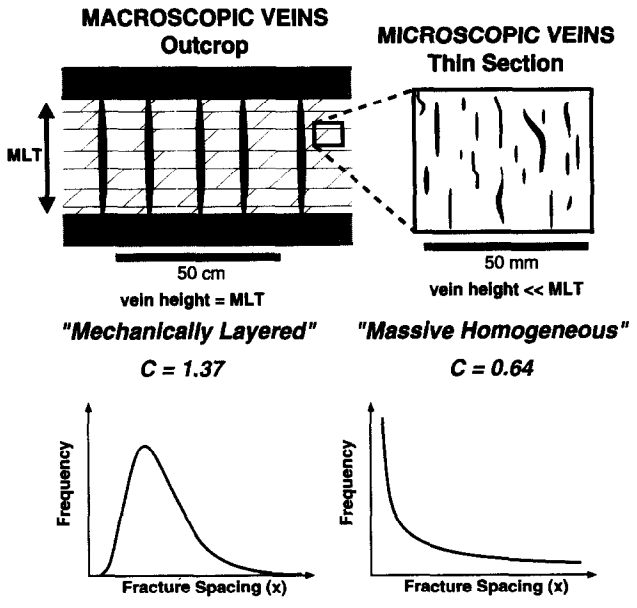

Fig. 14. Effect of scale and mechanical stratigraphy on vein spacing and aperture distributions in dolostone units of the Monterey Formation. Macroscopic veins are controlled by mechanical layering (MLT = mechanical layer thickness) resulting in a log normal spacing distribution and high C value, whereas microscopic veins behave as if in a massive homogeneous medium resulting in a power law spacing distribution and low C value.

scale-dependence of C derived from vein aperture population plots, and may in fact reflect the differences between vein propagation constrained by mechanical layer boundaries on the macroscopic scale and vein propagation uninhibited by mechanical layer boundaries on the microscopic scale.

Small normal faults within the mudstone mechanical unit account for only a small percentage of the total mudstone extension. The smaller faults are restricted to the organic-phosphatic-rich layers and do not cut through opal-CT beds. Consequently, although small faults may accommodate strain within intervals between opal-CT beds, they cannot contribute to opal-CT bed extension, and hence their contribution to overall extension of the mudstone unit is minimal. Indeed, variability in organic-phosphatic marl thickness as well as the presence of marl in fault zones are due in large part to movement along small extensional faults and the ductile nature of marl horizons. However, because opal-CT beds act as rigid plates within the mudstone unit they effectively inhibit the capacity of small marl-confined faults to accommodate the overall strain, thereby providing the means to calculate revised strain estimates from macroscopic fault displacements.

Bed normal vs bed parallel crack growth

An interesting pattern is observed in strain magnitudes measured from dolostone thin-section scanlines SL2 and SL3. In the two scanlines the mean strains for bed normal and bed parallel traverses are virtually identical (Fig. 10). However, in both instances bedding normal measurements exhibit a substantially wider variability in strain than measurements parallel to bedding, perhaps reflecting the more jagged paths taken by crack fronts as they encounter subtle lithologic changes across microscopic laminae (Fig. 9a). Crack fronts advancing parallel to bedding, on the other hand, intersect fewer obstacles, resulting in straighter vein walls and hence less variation in aperture width along their lengths (Fig. 9b).

Implications for development of western Transverse Ranges

Veins and faults in mechanical units at Arroyo Burro may shed some light on the complex tectonic development of the western Transverse Ranges. Cross-cutting relationships and fracture orientations imply these features are late-formed and related to Pliocene to recent northeast–southwest directed shortening. Furthermore, fault and vein alignment with present-day S_H derived from Quaternary fold development (Rockwell *et al.* 1988), earthquake focal mechanisms (Corbett & Johnson 1982), and borehole breakouts (Mount & Suppe 1992) strongly suggest fracture propagation post-dated the 90° clockwise rotation of the western Transverse Ranges determined from paleomagnetic studies (Hornafius 1985, Luyendyk 1991, Nicholson *et al.* 1994). Most importantly, the ~10% strain recorded by veins and faults in the dolostone and mudstone units attest to significant strike-parallel (NW–SE) extension accompanying development of the western Transverse Ranges fold and thrust belt.

CONCLUSIONS

Fracture strain estimates for adjacent mudstone and dolostone mechanical units at Arroyo Burro vary according to method of measurement and scale. However, adjusting strain estimates by means of fault displacement population analysis yields uniform displacement boundary conditions for both mechanical units. This identical fracture-related strain occurs despite differences in failure mode and lithologic composition between beds. Mechanical stratigraphy plays a major role in determining how strain is accommodated within interbedded units of the Monterey Formation. Whereas large faults account for the majority of extension in the mudstone unit at Arroyo Burro, microscopic veins provide a significant contribution to the overall dolostone strain. The presence of brittle opal-CT layers within the mudstone effectively controls the mechanical behavior of the mudstone, while vein distribution in the dolostone depends upon scale. In dolostone the dependence of vein spacing distributions and aperture population plots on scale suggest that lithologic boundaries control growth of outcrop-scale veins, whereas veins in thin section develop as if in a homogeneous medium. In addition, theoretical fault displacement population analysis is applicable for units that fail in effective tension in cases where vein apertures follow power-law distributions. The ~10% strain recorded at Arroyo

Burro attests to significant NW–SE strike-parallel extension accommodated by brittle failure during Pliocene to recent compression of the western Transverse Ranges.

Acknowledgements—We thank Wendy Bartlett for introducing us to the field area and assisting in data collection, and Don Fisher, Avrami Grader, Deane Smith and David Green for helpful discussions. Thoughtful reviews by Randall Marrett, John Lorenz, Marco Antonellini and James Evans greatly improved the manuscript. Funding for this project was provided by a research grant from Texaco Inc.

REFERENCES

Angelier, J. 1985. Extension and rifting: the Zeit region, Gulf of Suez. *J. Struct. Geol.* **7**, 605–612.

Angelier, J. 1994. Fault slip analysis and paleostress reconstruction. In: *Continental Deformation* (edited by Hancock, P. L.). Pergammon Press, Oxford, 53–100.

Belfield, W. C., Helwig, J., La Pointe, P. & Dahleen, W. K. 1983. South Ellwood oil field, Santa Barbara Channel, California, a Monterey Formation Fractured Reservoir. In: *Petroleum Generation and Occurrence in the Miocene Monterey Formation, California* (edited by Isaacs, C. M. & Garrison, R. E.). Pac. Sec. SEPM, 213–222.

Childs, C., Walsh, J. J. & Watterson, J. 1990. A method for estimation of the density of fault displacements below the limit of seismic resolution in reservoir formations. In: *North Sea Oil and Gas Reservoirs II* (edited by The Norwegian Institute of Technology). Graham and Trotman, London, 309–318.

Corbett, E. J. & Johnson, C. E. 1982. The Santa Barbara, California, earthquake of 13 August 1978. *Bull. seism. Soc. Am.* **72**, 2201–2226.

Dibblee, T. W., Jr. 1950. Geology of southwestern Santa Barbara County, California. *Bull. Calif. Div. Mines & Geol.* **150**.

Dibblee, T. W., Jr. 1966. Geology of the central Santa Ynez Mountains, Santa Barbara County, California, *Bull. Calif. Div. Mines & Geol.* **186**.

Dibblee, T. W., Jr. 1982. Regional geology of the Transverse Ranges Province of southern California. In: *Geology and Mineral Wealth of the California Transverse Ranges* (edited by Fife, D. L. & Minch, J. A.). South Coast Geological Society Guidebook **10**, 7–26.

Donnellan, A., Hager, B., King, R. W. & Herring, T. A. 1993. Geodetic measurement of deformation in the Ventura Basin region, southern California. *J. geophys. Res.* **98**, 21,727–21,739.

Gross, M. R. 1993. The origin and spacing of cross joints: examples from the Monterey Formation, Santa Barbara coastline, California. *J. Struct. Geol.* **15**, 737–751.

Gross, M. R. In press. Fracture partitioning: failure mode as a function of lithology in the Monterey Formatio of coastal Canada. *Bull. geol. Soc. Am.*

Hornafius, J. S. 1985. Neogene tectonic rotation of the Santa Ynez Range, Western Transverse Ranges, California, suggested by paleomagnetic investigation of the Monterey Formation. *J. geophys. Res.* **90**, 12,503–12,522.

Hornafius, J. S. 1994. Field trip road log to the Monterey Formation between Santa Barbara and Gaviota, California. In: *Field Guide to the Monterey Formation Between Santa Barbara and Gaviota, California* (edited by Hornafius, J. S.). Pacific Section AAPG **GB72**, 107–123.

Hoyt, D. H. 1976. Geology and recent sediment distribution from Santa Barbara to Rincon Point, California. M.S. Thesis, San Diego State University.

Huang, Q. & Angelier, J. 1989. Fracture spacing and its relation to bed thickness. *Geol. Mag.* **126**, 355–362.

Jackson, J. & Molnar, P. 1990. Active faulting and block rotations in the western Transverse Ranges, California. *J. geophys. Res.* **95**, 22,073–22,087.

Kakimi, T. 1980. Magnitude-frequency relation for displacement of minor faults and its significance in crustal deformation. *Bull. geol. Surv. Japan* **31**, 467–487.

King, G. & Cisternas, A. 1991. Geological faulting: Do little things matter? *Nature* **351**, 350.

Larsen, S. C., Agnew, D. C. & Hager, B. H. 1993. Strain accumulation in the Santa Barbara Channel: 1970–1988. *J. geophys. Res.* **98**, 2119–2133.

Luyendyk, B. P. 1991. A model for Neogene crustal rotations, transtension, and transpression in southern California. *Bull. geol. Soc. Am.* **103**, 1528–1536.

Luyendyk, B. P., Kamerling, M. J. & Terres, R. 1980. Geometric model for Neogene crustal rotations in southern California. *Bull. geol. Soc. Am.* **91**, 211–217.

Marrett, R. & Allmendinger, R. W. 1991. Estimates of strain due to brittle faulting. *J. Struct. Geol.* **13**, 735–738.

Marrett, R. & Allmendinger, R. W. 1992. Amount of extension on 'small' faults: An example from the Viking graben. *Geology* **20**, 47–50.

Mount, V. S. 1989. State of stress in California and a seismic structural analysis of the Perdido fold belt, Northwest Gulf of Mexico. Ph.D. Dissertation, Princeton University.

Mount, V. S. & Suppe, J. 1992. Present-day stress orientations adjacent to active strike-slip faults: California and Sumatra. *J. geophys. Res.* **97**, 11,995–12,013.

Namson, J. & Davis, T. 1988. Structural transect of the western Transverse Ranges, California: Implications for lithospheric kinematics and seismic risk evaluation. *Geology* **16**, 675–679.

Narr, W. & Suppe, J. 1991. Joint spacing in sedimentary rocks. *J. Struct. Geol.* **13**, 1037–1048.

Nicholson, C., Sorlien, C. C., Atwater, T., Crowell, J. C. & Luyendyk, B. P. 1994. Microplate capture, rotation of the western Transverse Ranges, and initiation of the San Andreas transform as a low-angle fault system. *Geology* **22**, 491–495.

Novoa, E., Shaw, J. & Suppe, J. 1994. Structural transect across the eastern Santa Barbara Channel (western Transverse Range) California. *Bull. Am. Ass. Petrol. Geol.* **78**, 672.

Olson, D. J. 1982. Surface and subsurface geology of the Santa Barbara-Goleta metropolitan area, Santa Barbara County, California. M.S. Thesis, Oregon State University.

Ramsay, J. G. & Huber, M. I. 1983. *The Techniques of Modern Structural Geology, Vol. 1. Strain Analysis*. Academic Press, New York.

Reed, R. D. & Hollister, J. S. 1936. *Structural Evolution of Southern California*. American Association of Petroleum Geologists, Tulsa.

Rockwell, T. K., Keller, E. A. & Dembroff, G. R. 1988. Quaternary rate of folding of the Ventura Avenue anticline, western Transverse Ranges, southern California. *Bull. geol. Soc. Am.* **100**, 850–858.

Savage, J. C., Prescott, W. H. & Gu, G. 1986. Strain accumulation in southern California. *J. geophys. Res.* **91**, 7455–7473.

Scholz, C. H. & Cowie, P. A. 1990. Determination of total strain from faulting using slip measurements. *Nature* **346**, 837–839.

Segall, P. 1981. The development of joints and faults in granitic rocks. Ph.D. Dissertation, Stanford University.

Segall, P. & Pollard, D. D. 1983. Joint formation in granitic rock of the Sierra Nevada. *Bull. geol. Soc. Am.* **94**, 563–575.

Shaw, J. H. & Suppe, J. 1994. Active faulting and growth folding in the eastern Santa Barbara Channel, California. *Bull. geol. Soc. Am.* **106**, 607–622.

Walsh, J. J. & Watterson, J. 1992. Populations of faults and fault displacements and their effects on estimates of fault-related regional extension. *J. Struct. Geol.* **14**, 701–712.

Walsh, J., Watterson, J. & Yielding, G. 1991. The importance of small-scale faulting in regional extension. *Nature* **351**, 391–393.

Yeats, R. S. 1983. Large-scale Quaternary detachments in Ventura basin, southern California. *J. geophys. Res.* **88**, 569–583.

Yerkes, R. F. 1985. Geologic and seismologic setting. In: *Evaluating Earthquake Hazards in the Los Angeles Region — An Earth Science Perspective* (edited by Ziony, J. I.). *Prof. Pap. U.S. Geol. Surv.* **1360**, 25–42.

Zoback, M. D., Zoback, M. L., Mount, V. S., Suppe, J., Eaton, J., Healy, J. E., Oppenheimer, D., Reasenberg, P., Jones, L., Raleigh, C. B., Wong, I. G., Scotti, O. & Wentworth, C. 1987. New evidence on the state of stress of the San Andreas fault system. *Science* **238**, 1105–1111.